

Effects of annealing and specimen geometry on dynamic compression of a Zr-based bulk metallic glass

George Sunny

Department of Mechanical and Aerospace Engineering, Case Western Reserve University, Cleveland, Ohio 44106-7222

John Lewandowski^{a)}

Department of Materials Science and Engineering, Case Western Reserve University, Cleveland, Ohio 44106-7222

Vikas Prakash^{b)}

Department of Mechanical and Aerospace Engineering, Case Western Reserve University, Cleveland, Ohio 44106-7222

(Received 2 July 2006; accepted 4 October 2006)

High strain-rate compression experiments were performed with a split-Hopkinson pressure bar (SHPB) at 500–4000/s on cylindrical samples of a Zr-based bulk metallic glass (LM-1) in both the fully amorphous and annealed conditions. The effects of changes to the specimen geometry (i.e., L/D ratio) and the material heat treatment [i.e., annealing versus amorphous (as-received)], on the peak stress, strain-to-failure, and failure behavior were determined with the aid of an in situ video obtained by using a high-speed digital camera in conjunction with the split-Hopkinson pressure bar (SHPB). Examination of the in situ video recordings and light optical microscopy showed that the failed samples revealed preferential failure initiating at the sample ends due to stress concentration at the sample-insert interface. A new insert design was developed using transient, elastic-plastic finite-element simulations to reduce the effects of these stress concentrations. SHPB testing, combined with in situ video, subsequently revealed that this new experimental configuration promoted failure within the gage length and away from the sample ends in the samples tested. Significant effects of specimen geometry, insert design, and annealing on the apparent values of the peak stress, strain-to-failure, and fracture behavior were exhibited.

I. INTRODUCTION

Liquidmetal-1 (LM-1, $\text{Zr}_{41.25}\text{Ti}_{13.75}\text{Cu}_{12.5}\text{Ni}_{10}\text{Be}_{22.5}$) is a bulk metallic glass that can be processed to fully amorphous conditions in large thickness (e.g., 10–20 mm) because of its low critical cooling rate (e.g., 1 K/s). This material exhibits near theoretical strength and large elastic strains (~2%) under quasi-static loading,¹ along with remarkably high toughness in both notched and fatigue-precracked conditions.²

Relatively few authors have investigated the high strain-rate behavior of Zr-based bulk metallic glasses (BMGs). Early studies on $\text{Zr}_{41.25}\text{Ti}_{13.75}\text{Ni}_{10}\text{Cu}_{12.5}\text{Be}_{22.5}$

revealed similar peak strengths under dynamic and quasi-static conditions for both cylindrical and parallel-piped specimens, with failure characterized by inhomogeneous flow via locally intense shear.^{3,4} More recent work on both $\text{Zr}_{57}\text{Ti}_5\text{Cu}_{20}\text{Ni}_8\text{Al}_{10}$ and $\text{Zr}_{41.25}\text{Ti}_{13.75}\text{Ni}_{10}\text{Cu}_{12.5}\text{Be}_{22.5}$ has reported negative strain-rate sensitivity.^{5,6} Similar behavior was also reported for BMGs when Hf was used to replace Zr.⁷

The materials investigated in the previous experiments^{2–7} were in the as-cast (i.e., fully amorphous) condition. All of the experiments exhibited failure via formation of a single dominant shear plane. Some of the experiments on fully amorphous LM-1 revealed an increase in failure strain with increased strain-rate,^{6,8} while the extent of sample fragmentation after shear failure was also observed (via high-speed photography) to increase with increasing strain-rate in one high-rate study.⁶ Annealing of LM-1 to reduce the free volume has been shown to produce slight increases in strength but significant embrittlement via a loss in toughness^{9–11} under quasi-static conditions. This embrittlement and change in

^{a)}This author was an editor of this focus issue during the review and decision stage. For the *JMR* policy on review and publication of manuscripts authored by editors, please refer to http://www.mrs.org/jmr_policy.

^{b)}Address all correspondence to this author.

e-mail: vikas.prakash@case.edu

DOI: 10.1557/JMR.2007.0042

fracture characteristics has recently been correlated with changes to the material's elastic constants¹² that accompany either annealing or changes in chemistry. Little work has been conducted on the effects of annealing on the high strain-rate behavior.

In this work, the effects of both specimen aspect ratio (i.e., L/D) and annealing on the high strain-rate compressive behavior of LM-1 are investigated using cylindrical samples and the conventional split-Hopkinson pressure bar (SHPB) in the Department of Mechanical and Aerospace Engineering at Case Western Reserve University. In situ high-speed video recordings were analyzed to determine the effects of these changes on the modes of dynamic deformation and failure. In addition, a new insert design was devised to reduce the stress concentration at the specimen-insert interface. In situ video during SHPB testing was examined to determine the effects of the reduced stress concentration on the deformation and failure of the fully amorphous specimens using the new insert-specimen design combination.

II. MATERIALS AND METHODS

The material used in the present study was LM-1, supplied by Liquidmetal, Inc. (Lake Forest, CA) in the form of rectangular plates of dimensions 90 mm × 63 mm × 5 mm. These plates were determined to be fully amorphous by differential scanning calorimetry (DSC) and x-ray diffraction (XRD) in previous work.^{2,11,13} The plates were then electrical-discharge machined into rectangular bars and subsequently ground to cylindrical bars of diameter 3.2 mm or 4.0 mm. The long cylindrical bars were then metallographically polished to a mirror finish via a combination of SiC grit paper and diamond paste. Right cylindrical specimens with aspect ratios of 0.5, 1.0, and 2.0 were then prepared by slicing the bars with a low-speed saw (Buehler, model 11-1180) so that the faces were flat and parallel. The faces were then lapped and polished to a 6- μ m finish before testing. Some of the polished cylindrical samples were annealed at 623 K (the glass transition temperature of the metallic glass) for 12 h and then air-cooled to reduce the free volume without inducing full crystallization.^{11,12,14} This temperature was chosen

because of previous work that showed a slight increase in strength after annealing at 623 K for 12 h¹⁴ but a dramatic reduction in toughness.^{11,12,14} Both XRD and DSC analyses of the fully amorphous and annealed materials have been characterized previously.¹⁴ Finally, the faces of the annealed samples were again lapped and polished to remove any oxide layer that may have formed during annealing.

The SHPB (Fig. 1), reviewed elsewhere,¹⁵ was used to determine the dynamic stress-strain response. The SHPB at Case consists of an air-pressurized gas gun and three 19.05 mm diameter maraging steel bars—a striker (20 mm), an incident bar (1.6 m), and a transmitted bar (1.5 m). Semiconductor strain gages (Vishay BLH, model SR-4, Raleigh, NC) were placed on both the incident and transmitted bars. Because of their high gage factor, these gages have a very high signal-to-noise ratio, minimizing the amount of amplification required. Both strain gages were used in combination with a Wheatstone bridge circuit connected with a differential amplifier (Tektronix 5A22N) and a high-bandwidth digital oscilloscope (Tektronix TDS 680C). The recorded reflected and transmitted signals can be used to determine the stress, strain-rate, and strain¹⁵ via accepted procedures. Strain-rates varying from 500/s–4000/s were obtained depending on the striker bar velocity utilized, which ranged from 5 m/s–15 m/s.

Impedance-matched maraging steel inserts bonded to the incident and transmitted bars with vacuum grease were utilized to prevent denting of the incident and transmitted bars. Molybdenum disulfide grease was utilized between the inserts and the specimen to ensure low friction at the specimen-insert interfaces.

Because of the limited strain-to-failure of the bulk metallic glass, a copper pulse shaper was used to control the shape (rise-time) of the incident pulse and thus promote equilibrium conditions within the specimen.¹⁶ In general, the pulse shapers used in the present study were ~5–10 mm on the side and 0.2–0.7 mm thick. Figure 2(a) shows typical incident and transmitted signals of samples tested using a copper pulse shaper. As seen from Fig. 2(b), a nominally constant strain-rate of 450/s is obtained for true strains of 0.01–0.03.

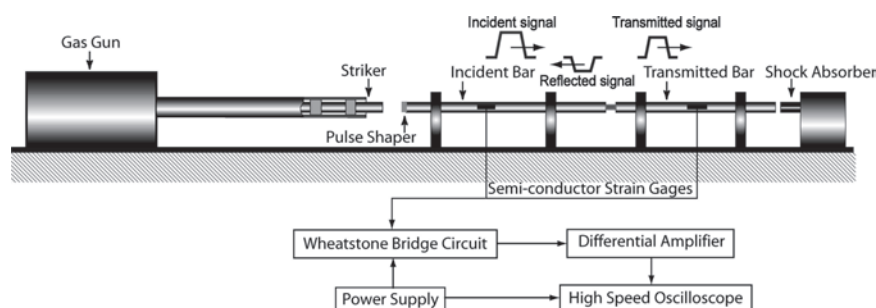


FIG. 1. Schematic of the Split-Hopkinson Bar¹⁵ used for high strain-rate compression.

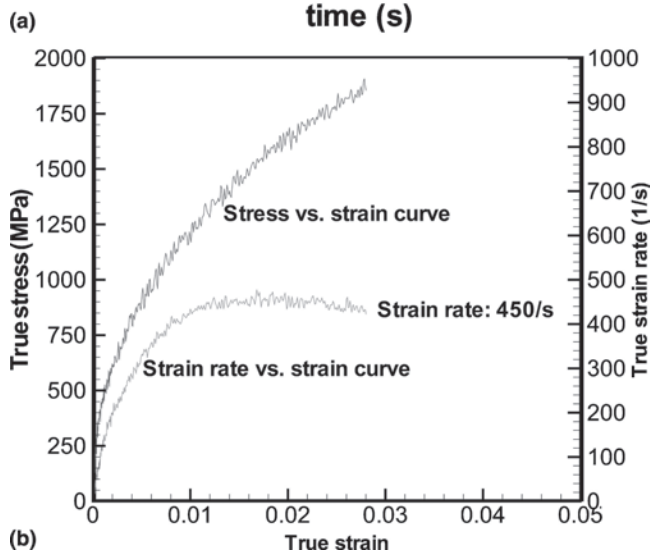
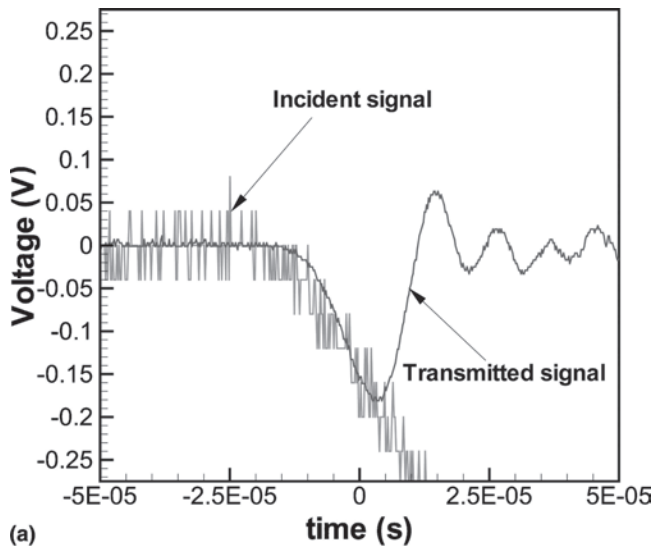


FIG. 2. Comparison of slopes of (a) incident and transmitted signals and (b) corresponding stress–strain curve and constant strain-rate regime.

An ultra-high-speed camera (IMACON 200, DRS Technologies, Inc.) was used to perform in situ video recording of the deformation and failure process. Sixteen pictures were taken for each specimen, with inter-frame times of 5–7 μs and an exposure time of 1 μs . The in situ video was examined to determine the dynamic failure modes in the BMG specimens in both the amorphous and annealed conditions.

III. RESULTS: CYLINDRICAL INSERTS

A. Effect of changes in aspect ratio on fully amorphous LM-1

Representative true-stress versus true-strain are shown in Fig. 3(a) for the amorphous specimens with L/D ratios of 0.5 and Fig. 3(b) 2.0. In general, the specimens with a

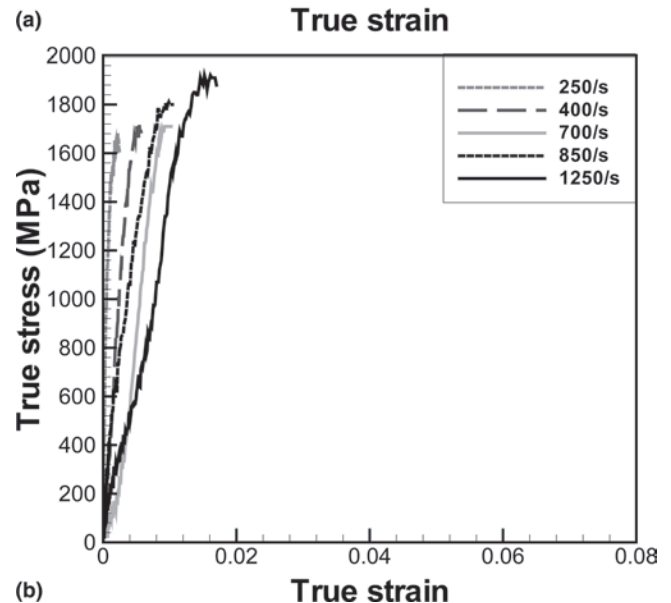
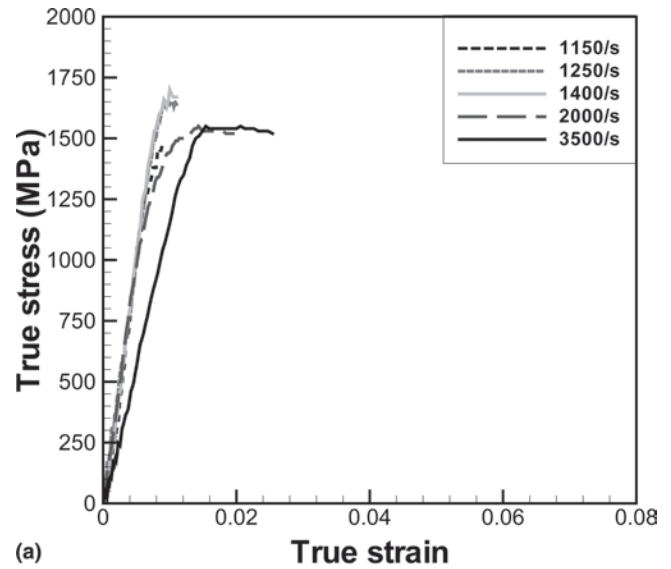


FIG. 3. Stress–strain curves for specimens of L/D ratio (a) 0.5 and (b) 2.0.

higher aspect ratio exhibit higher apparent peak stresses but lower observed strains-to-failure.

Figure 4 shows sequential images from the high-speed camera of an amorphous specimen with $L/D = 1.0$. While the specimen is loaded, a shear instability forms in the specimen [Fig. 4(b)], which apparently starts at the sample-insert interface as determined by analyses of the fracture sample. This leads to the formation of a dominant fracture plane [Fig. 4(c)], and the specimen fractures into two discrete pieces. These fractured pieces slip relative to each other [Fig. 4(d)]. Such behavior was consistently exhibited for specimens with $L/D = 1.0$ and 2.0, while optical analysis of the samples revealed that fracture initiated at the sample-insert interface.

For an aspect ratio of $L/D = 0.5$, due to the shorter length of the specimen, the dominant shear plane is

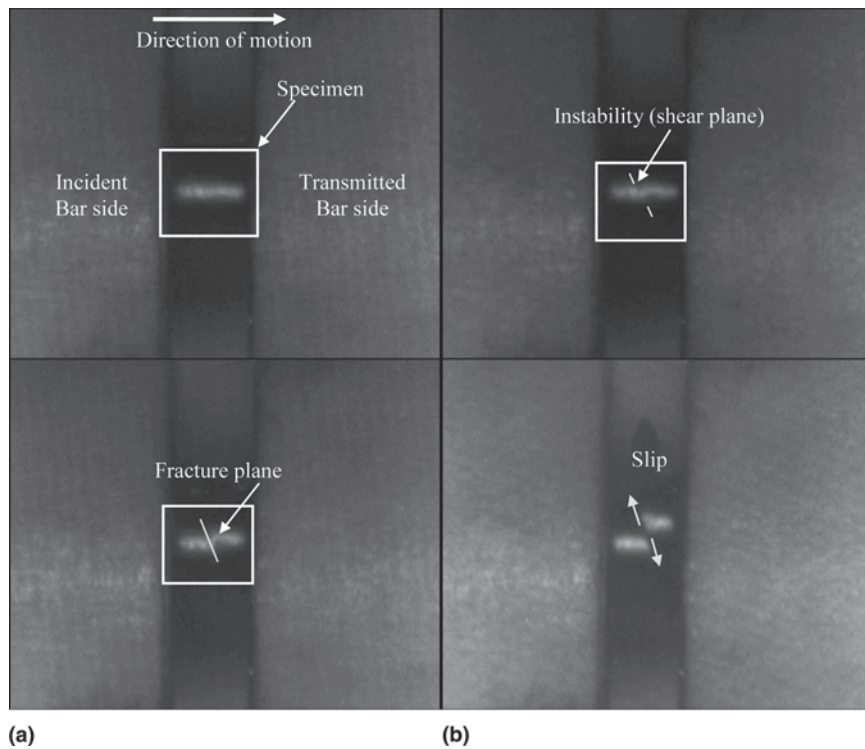


FIG. 4. Sequential images of amorphous LM-1 obtained from a high-speed video. (a) Undeformed specimen, (b) formation of shear plane, and (c, d) material failure at strain-rate of 800/s are illustrated here. Light optical microscopy of these samples revealed that failure started at the sample-insert interface.

located such that it intersects the specimen at the two specimen-insert interfaces, thus inhibiting catastrophic failure of the specimen by the formation of a macroscopic shear plane instability observed in experiments with the longer length specimens (with $L/D = 1.0$ and/or $L/D = 2.0$). Fig. 5 shows sequential images from the high-speed camera for an amorphous specimen with $L/D = 0.5$. The specimen exhibits the formation of a shear plane during the dynamic loading process [Fig. 5(b)] between the incident and transmitted bars; however, the fractured pieces are trapped between the inserts and continue to support the load; this is reflected in the increased strain-to-failure observed in these experiments. Figure 6 illustrates the difference between the two large ($L/D = 1.0, 2.0$) and small ($L/D = 0.5$) aspect ratios: specimens with higher L/D ratios fracture into discrete pieces after specimen failure [Fig. 6(a)]; those with lower L/D ratios appear to exhibit more fragmentation and subsequent crushing/consolidating behavior [Fig. 6(b)]. Fracture angles for the higher aspect ratio specimens were about 50 degrees, in agreement with previous work,^{11,13,14} although close analysis of the sample shown in Fig. 6(a) reveals that the fracture appeared to initiate from the sample-insert interface.

B. Effects of annealing of LM-1

Representative stress-strain curves are shown in Fig. 7 for both the annealed and fully amorphous material for

L/D ratios of 1.0 and 2.0. In general, the annealed material exhibited equal or higher strength when compared to the as-cast material, but there is some scatter in the peak stresses. The data suggest that the annealing treatment did not reduce the strain-to-failure for $L/D = 1.0$, but dramatically increased the observed strain-to-failure for specimens with $L/D = 2.0$.

The deformation process of the metallic glass during dynamic compression appears to change drastically when the material is annealed. Figure 8 shows a typical deformation and failure process for an annealed specimen. In the first frame, a shear band forms [Fig. 8(a)], which appears to be caused by a geometrical instability that starts at the sample-insert interface. Immediately after the formation of the shear band, the specimen begins to shatter into multiple fragments [Fig. 8(b) and 8(c)] and is eventually pulverized. The extent of fragmentation is far more extensive than that exhibited by the amorphous LM-1 (Fig. 5).

IV. DESIGN OF NEW INSERTS

The observation of preferential failure near the specimen-insert interface strongly suggests the presence of a large stress concentration in this region. In the analysis of split-Hopkinson bar experiments, there are five assumptions¹⁷ that lead to the equations for stress and strain-rate. One of these assumptions, the uniform and uniaxial stress state, is difficult to achieve because the diameters of the

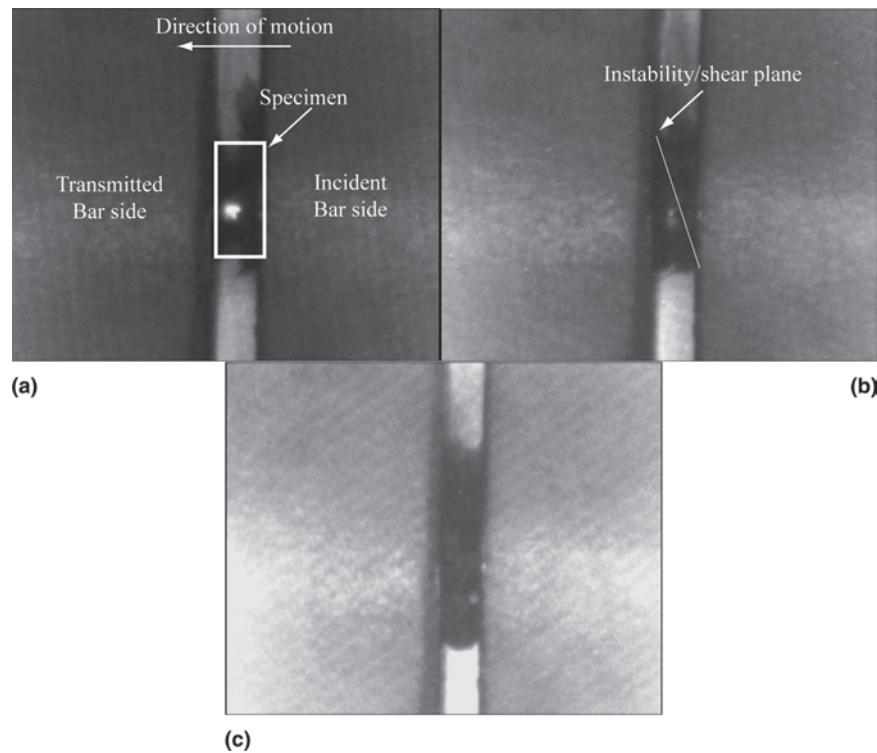


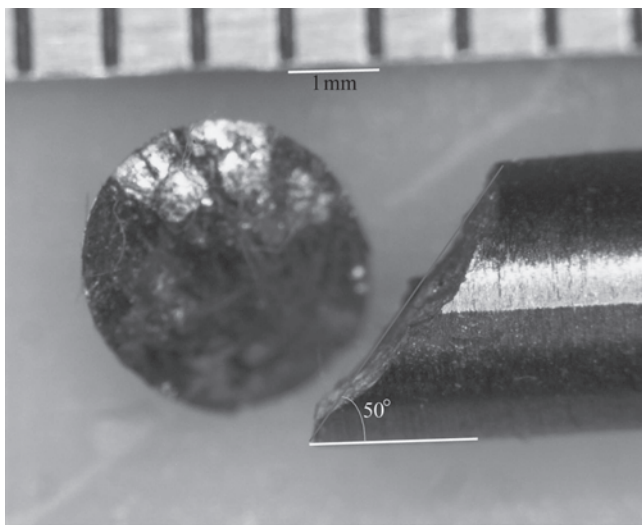
FIG. 5. (a) Sequential images showing undeformed amorphous LM-1, (b) shear plane formation, and (c) failure at strain-rate of 2000/s.

insert and the specimens do not match, resulting in a stress concentration in the specimen. This behavior has been noted before in ceramics,¹⁸ where the stress concentration was estimated to be 1.75.

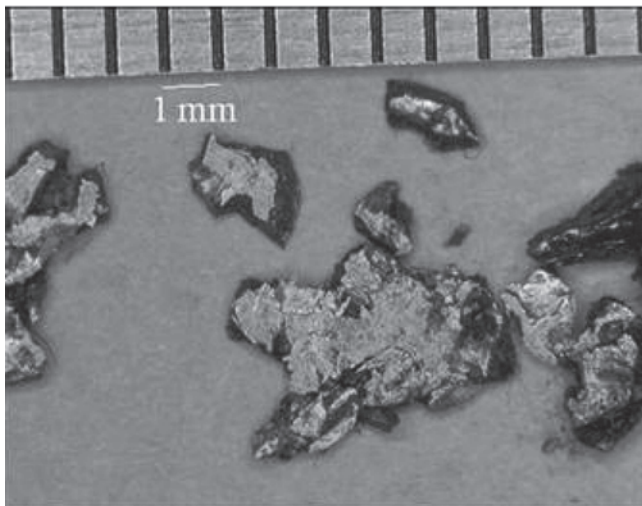
To determine qualitatively the effects of stress concentration on conventional SHPB specimens, finite element simulations (LS-DYNA) were performed to determine the stress state in the specimen during the dynamic loading process. Axisymmetric finite elements were used to model the disk shaped specimens used in the present experiments; the radius is 1.6 mm to replicate the initial conditions of the experiments. Appropriate stress and particle velocity boundary and initial conditions were prescribed to represent accurately the dynamic loading on the specimens using the SHPB apparatus. Mesh sizes were 0.05 mm along the radial direction and were graduated from 0.05 mm in the specimen and the specimen-insert interface to 1.7 mm at the ends of the transmitted and incident bars in the axial direction. The BMG was assumed to be bilinear elastic-plastic with plastic modulus of 0.1 E, which is consistent with the nearly perfectly elastic-plastic behavior exhibited by the BMG under both quasi-static and dynamic loading conditions.³ The Young's moduli for the bar and the specimen were taken to be 210 GPa and 96 GPa, respectively. Profiles of the axial and in-plane shear stresses were developed for each of the three L/D ratios, and the planes of maximum shear stress¹⁹ were determined to gain insight into the failure mechanisms. Figure 9(a) shows a schematic of the finite

element simulations along with the axial stress contours for the different aspect ratios [Fig. 9(b)]. These results are presented at the time of failure obtained from the experiments for each of the three L/D ratios. For all three aspect ratios significant deviations (greater than 10%) are observed in the uniaxial state of stress, with stresses being the highest along the lateral boundary nearest the inserts and much lower near the axis of symmetry. This lack of uniformity was particularly prevalent in specimens with $L/D = 0.5$; while the stress along the lateral boundary exceeded the yield stress of LM-1 (2 GPa), the stress near the axis of symmetry was 30% lower. The average stress in the specimen at the time of failure is lowest for the smallest specimens, which may explain the observed reduction in strength with aspect ratio for the fully amorphous samples shown in Fig. 3. In addition, the progressively lower times for failure, due to the stress reaching the critical failure stress level of the BMG as the loading rate is increased, lead to lower average axial stresses in the specimen at the time of failure, and may partially explain the negative strain-rate sensitivity that has been previously reported in both LM-1 and LM-106 at high strain-rates.⁵

Because of the large discrepancy between the stresses on the lateral boundary and on the interior of the specimen, a new insert design was developed to reduce the stress concentrations that are present in the present experimental setup. "Dog-bone" compression specimens^{17,18} have both been analyzed for their feasibility in



(a)

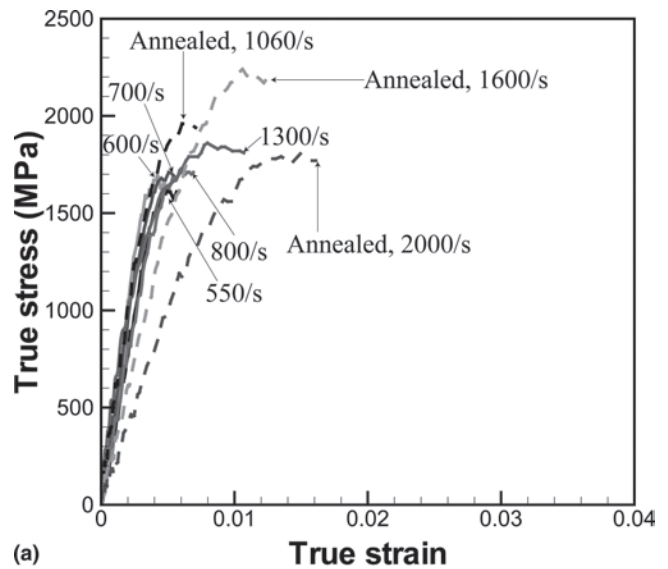


(b)

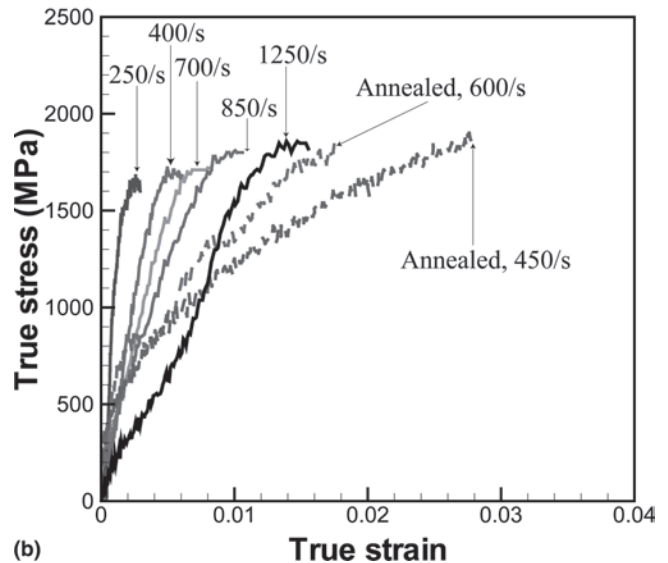
FIG. 6. Representative images of LM-1 after failure for aspect ratios of (a) 1.0 and 2.0 and (b) 0.5.

SHPB testing, and, aside from the cost and difficulty of machining, have been viable approaches to this issue. However, the testing of LM-1 produces an additional challenge: ensuring uniform material properties for this bulk metallic glass is quite difficult when the diameter exceeds 10 mm. The slower cooling rates at the center of castings may result in the loss of free volume and/or crystallization, thereby changing the material properties, as clearly shown elsewhere.^{10–12} Machining costs may also be prohibitive. In addition, as seen in Fig. 10(a), there is a region of shear stress in the area where the dog-bone specimen changes diameter, and this region, coupled with the very high axial stresses that are present [Fig. 10(b)], may cause failure outside of the gage region.

To reduce the possibility of failure outside the gage region, a design replacing the ends of the dog-bone



(a)



(b)

FIG. 7. Dynamic stress-strain curves for annealed (dashed) and as-received (solid) LM-1 for L/D ratios of (a) 1.0 and (b) 2.0.

with a high-strength steel was developed. Maraging steel (Vascomax C350, Allvac Metals, Monroe, NC) with yield strength 2.5 GPa was utilized to ensure failure occurs in the BMG specimen before insert damage. Figure 11(a) shows shear and Fig. 11(b) axial stress contours for this experimental setup, which shows that the peak stress of the maraging steel insert is no more than 15% more than that of the bulk metallic glass, so specimen failure should occur before insert failure.

After machining, the inserts were lapped at the bar interface and surface ground and polished at the specimen interface. The maraging steel inserts were then aged at 783 K for 6 h to increase the strength of the maraging steel inserts to peak values of stress (e.g., 2.5 GPa) and hardness (e.g., $HR_c = 60$) and then were lapped, surface ground, and polished again to remove any oxide layer produced during aging.

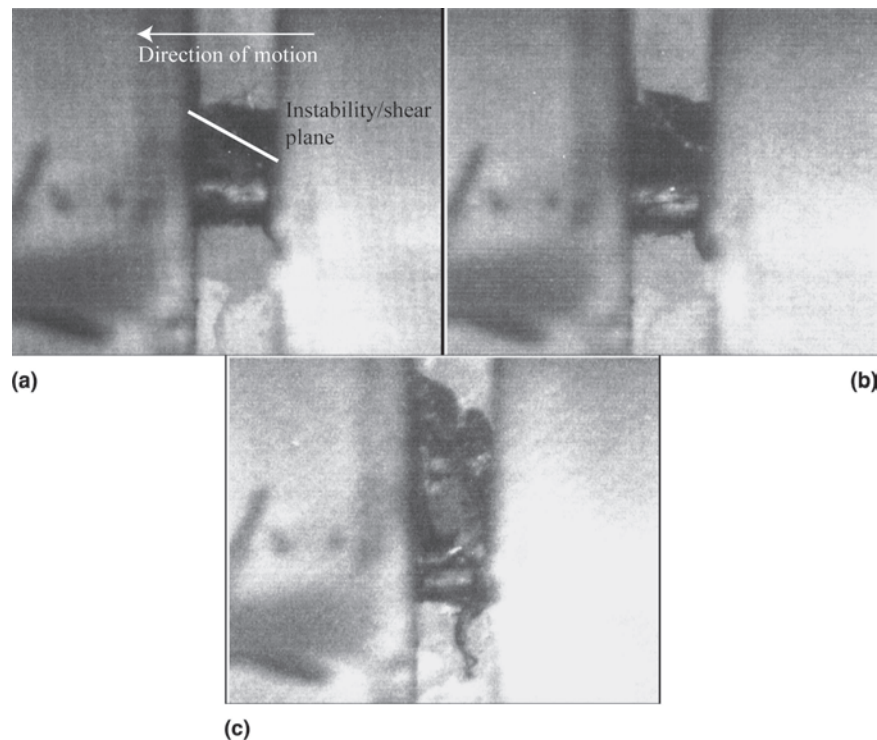


FIG. 8. (a, b) Sequential images of deformation, failure, and (c) fragmentation of annealed LM-1 at strain-rate of 1600/s.

V. SPLIT-HOPKINSON PRESSURE BAR RESULTS OBTAINED WITH NEW INSERTS

The amorphous LM-1 exhibits different fracture behavior when tested with the new inserts. Figure 12(a) shows the specimen along with the inserts, as seen from the high-speed camera before impact. Specimens with an L/D ratio of 1.0 appear to exhibit an initial instability initiating from the periphery of the specimen resulting in the formation of a shear plane between the initial instability and the middle of one of the two faces, leading to failure (fragmentation) of the specimen [Fig. 12(b)]. The smaller fragments are ejected [Figs. 12(c) and 12(d)] and the remaining sample impacts the insert. This is notable because the location of the initiation of failure is away from the region of stress concentration (periphery of the cylindrical specimen in contact with the loading faces) as was the case in the dynamic experiments conducted using the conventional SHPB discussed earlier. As-cast LM-1, with an L/D ratio of 2.0, also appears to exhibit such instability in the gage section. For all of the experiments, the inserts were damaged after the fracture of the BMG, due to the impact of the fractured specimen on the loading faces.

VI. DISCUSSION

A summary of the results from the experiments in the present study is shown in Table I. When the L/D ratio is reduced from 1.0 or 2.0 to 0.5, the peak stress is reduced

because of the shorter time to failure, but the apparent strain-to-failure is increased because of the geometrical constraint provided by the incident and transmitted bars, leading to crushing behavior. When the specimen is annealed at 623 K, the peak stress is increased slightly, and the apparent strain-to-failure is increased because of damage accumulation in the specimen before fragmentation. Use of the new inserts promotes self-sharpening behavior of the BMG, but as is discussed later, it is not possible to determine accurate peak stresses and strains-to-failure because of dispersion effects due to the new inserts.

A. Mechanistic and thermal effects in LM-1

The present results are generally in agreement with other recent data generated at high strain-rates^{5,6} showing an apparent negative strain-rate sensitivity. However, the present study has investigated a wider range of L/D than used in the previous studies of amorphous LM-1 and finds that an even greater negative strain-rate sensitivity is exhibited by samples with smaller L/D ratios. This observation suggests that the presently observed L/D effects and the resulting stress concentrations at the sample-insert interface are the key source for the reduced yield stress with increasing strain-rates in the SHPB experiments.

One commonly proposed interpretation of the negative strain-rate sensitivity during dynamic deformation of materials has been thermal softening, which manifests itself

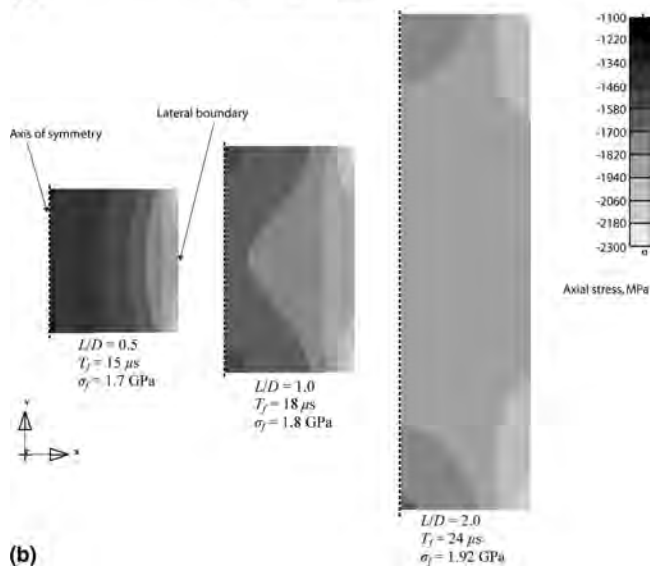
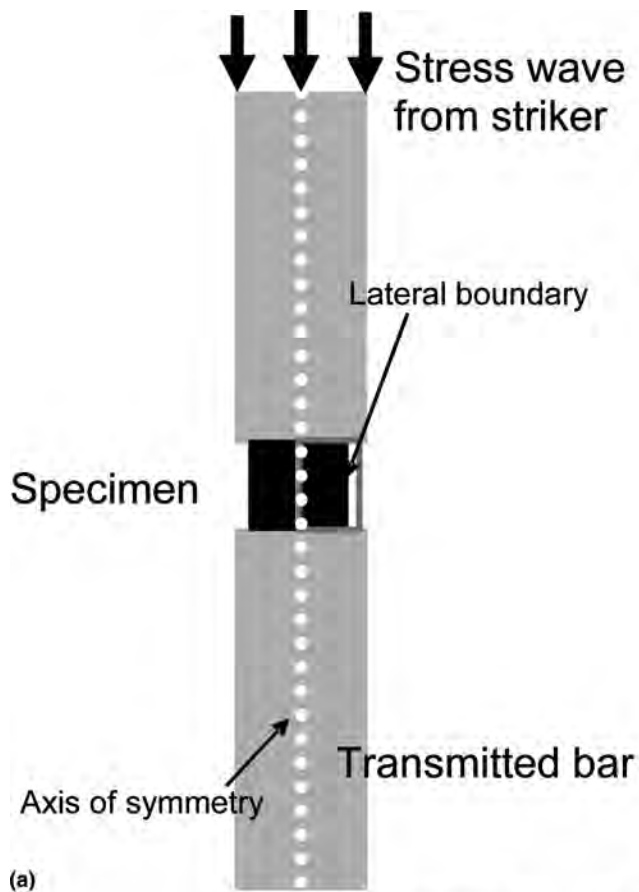


FIG. 9. Schematic of (a) finite element simulation and (b) the axial stress contours at the time of failure obtained from the experiment.

from the competition between adiabatic heating and thermal conductivity.⁵ However, a significant temperature rise in the BMG specimens cannot occur during a typical dynamic loading process because failure of the specimen is consistently observed to occur before significant plastic flow can accumulate in the specimen. Early work,³

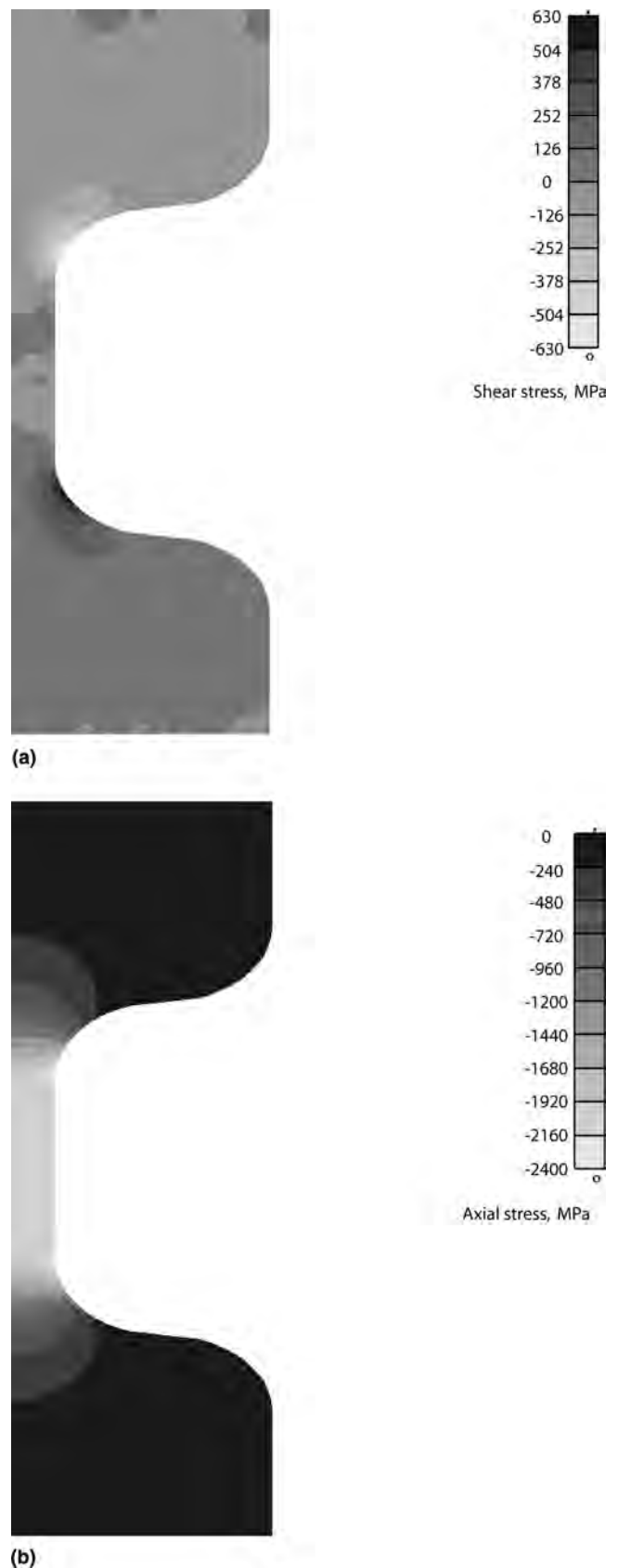


FIG. 10. LS-DYNA simulation of (a) shear and (b) axial stress contours for a dog-bone specimen of one material.

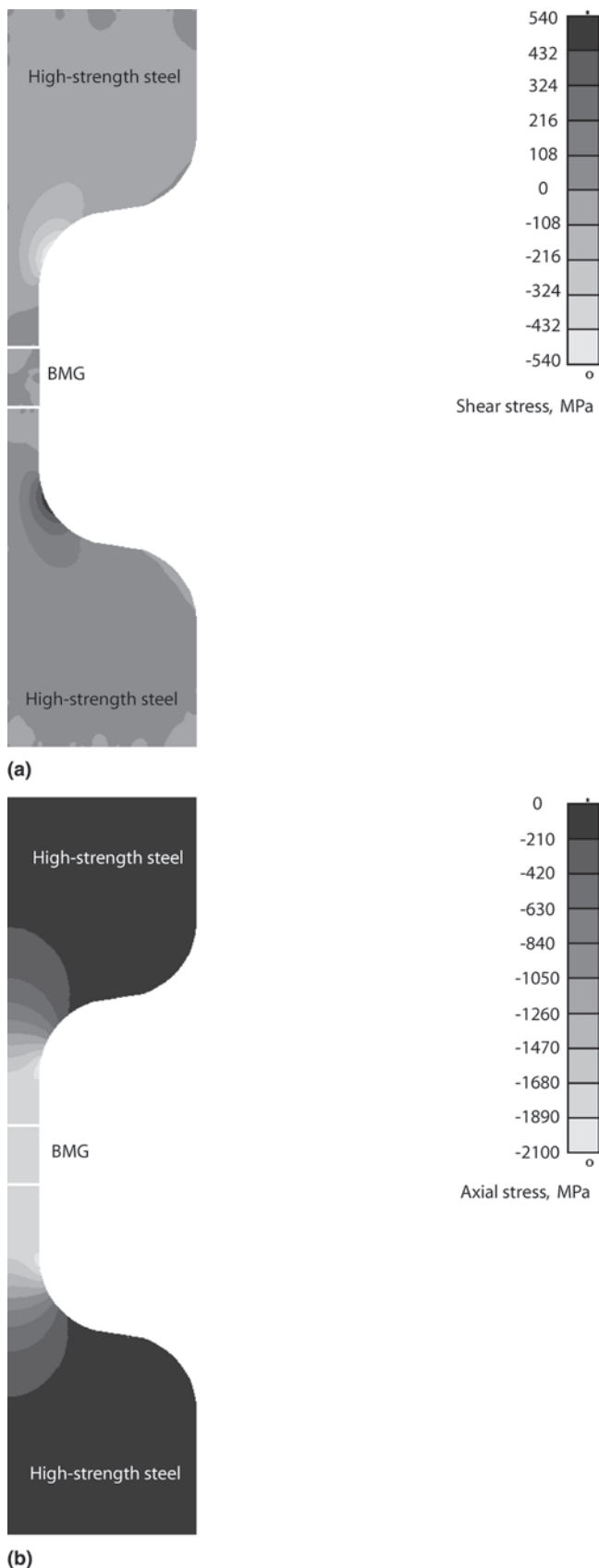


FIG. 11. FEM simulations of (a) shear and (b) axial stress contours with new insert design.

which used infrared temperature detection, has revealed a significant temperature rise at the fracture plane during the dynamic failure, and other works^{9,20} show a temperature rise at the fracture plane at the point of final failure. More recent work²¹ using fusible coatings that can provide a high spatial and temporal resolution clearly shows that the magnitude of the temperature rise in the specimen is associated with the magnitude of the shear offset (amount of plastic flow/slip on the fracture/shear plane) in the fracture plane, as well as other material properties including the dynamics of the shear band. This suggests that the drop in peak stress with increasing strain-rate for these experiments is not due to the temperature rise in the specimen. Moreover, recent detailed analyses further indicate that shear banding in these BMGs is not due to adiabatic events.^{21–23}

The previous discussion indicates that exploring the effects of changes in L/D ratio on the magnitude of the peak stress, as well as the effects of stress concentrations at the sample-insert interface is relevant. Reducing the L/D ratio from 2.0 to 0.5 clearly reduces the magnitude of the peak stress obtained in the fully amorphous material. FEM calculations of the stress concentration clearly showed a higher stress concentration at the specimen boundaries in the $L/D = 0.5$ sample compared with the $L/D = 2.0$ sample. Furthermore, high-speed video and analysis of the failed samples clearly showed preferential flow/fracture from the sample-insert interface in all of the as-cast BMG samples tested with the conventional inserts, which had significant geometry and property differences when compared with the specimen. The new insert design was developed with the finite element method (FEM) analysis to reduce this stress concentration, and hence premature failure of the specimens. The in situ video of as-cast samples clearly showed that these new inserts promoted failure in the gage section of the sample in regions well removed from the sample-insert interface. While for the as-cast LM-1 the number of fracture planes is unchanged from the previous experiments, the fracture planes are orientated in such a way that they promote self-sharpening behavior of the material and penetration of the sharpened bulk metallic glass into the insert.

B. Additional considerations with new insert design

Such behavior has motivated the development of Zr-based bulk metallic glass composites for anti-armor applications by increasing the density while taking advantage of the self-sharpening behavior. Unfortunately, the stress-strain curves could not be obtained from these samples yet because the new inserts, although not producing significant stress concentrations, do lead to significant dispersion of the stress waves because of the non-uniform cross-sectional area of the insert, so the

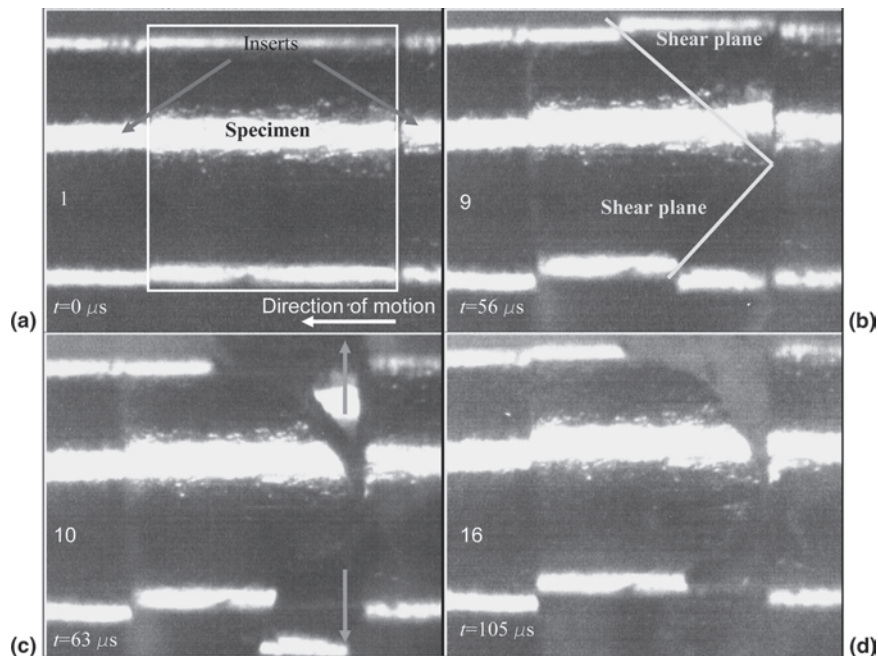


FIG. 12. (a) Sequential images of as-cast LM-1 specimen ($L/D = 1$) with new inserts at strain rate 3000/s, including (b) shear plane formation, (c) sample failure, and (d) subsequent impact with the insert.

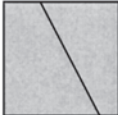

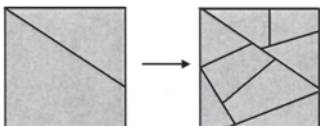

strain-rate and strain cannot be obtained directly from the incident and transmitted bar strain gage signals. To remedy this issue, strain gages must be placed directly on the specimen and a linear elastic stress-strain curve must be assumed. Previous quasi-static work^{11,14} conducted on highly aligned samples of $L/D = 2.0$ suggests that the stress-strain relationship is indeed linear, so this is a valid assumption. Another way to compensate for dispersion in the signals involves the use of explicitly determined dispersion relationships, such as the Pochhammer-Chree relation. However, obtaining closed-form dispersion relations in complicated waveguides, such as the new inserts, may not be possible. Now that the failure in the gage section has been promoted, investigation of the use of strain gages on the specimen is presently being conducted to determine whether or not there actually is an effect of L/D ratio or strain rate on the peak strength of LM-1 in both the amorphous and annealed conditions.

Although the present study focused on a new design for determining the material behavior of a bulk metallic glass under high strain-rate uniaxial compression, these inserts can also be used in tests investigating the material behavior of other materials with low strains-to-failure, such as ceramics, under dynamic uniaxial loading conditions. In both the bulk metallic glass and the ceramic, the stress concentrations normally present when cylindrical inserts are used may be virtually eliminated when the new inserts are used. This also potentially eliminates the need to use dog-bone compression samples,^{16,17} which are difficult to machine, and because maraging steel before annealing is machinable ($HR_c = 33$), the production

of multiple inserts is both less time consuming and less costly.

In addition to the previous discussion, reducing the L/D ratio in the fully amorphous material tested at high strain-rates appears to increase the strain-to-failure without changing the mechanisms of flow, which again occurred via shear. Increased compressive ductilities with reduced L/D have been reported previously in quasi-static tests conducted on LM-1 at atmospheric pressure,^{11,13,14,24} as well as with the superimposition of pressure.^{11,13,14} The quasi-static results obtained on LM-1 at atmospheric pressure are consistent with the effects of reduced L/D on the behavior of semibrittle and brittle materials, demonstrated decades ago.²⁵ In those works, the increased compressive ductilities that accompanied the reduced L/D ratios was explained as due to the increased effective pressure and constraint that accompanies the reduced L/D . The increased compressive ductilities obtained with reduced L/D on LM-1 obtained by Bruck and colleagues²⁴ were similarly explained, while the high pressure results^{11,13,14} clearly showed that increasing the level of hydrostatic pressure in compression tests was very effective in increasing the compressive ductility, even in samples tested with $L/D = 2.0$, although the flow stresses were not very pressure-dependent at room temperature. The present work showing increased compressive ductility with decreasing L/D is generally consistent with all of the quasi-static tests described previously, while the in situ video provides direct evidence of the events that contribute to the increased ductility in compression at high loading rates

TABLE I. Results from experiments.

Material/insert	Peak stress	Apparent strain-to-failure	Fractured sample appearance (from camera)
Amorphous, $L/D = 1.0$ or 2.0 cylindrical insert	~ 1.8 GPa	$\sim 1\text{--}2\%$	
Amorphous, $L/D = 0.5$ cylindrical insert	< 1.8 GPa	$> 1\text{--}2\%$	
Annealed, cylindrical insert	> 1.8 GPa	$> 1\text{--}2\%$	
Amorphous, tapered insert	N/A	N/A	

when the L/D ratio is reduced. The fragmentation and subsequent consolidation appear to provide a potent energy-absorbing mechanism with decreasing L/D for fully amorphous LM-1.

C. Effects of annealing

The annealing treatment presently used clearly produces a change in the failure mechanism of LM-1. While previous work has clearly demonstrated embrittlement via significant reductions to the fracture toughness via this annealing treatment,^{11,12,14} the quasi-static compressive strengths and hardness were somewhat increased via this annealing treatment.¹⁴ Interestingly, under high strain-rate conditions, the annealed LM-1 also exhibits a somewhat increased strength and strain-to-failure in comparison to the fully amorphous LM-1. The high-speed video recording clearly shows multiple fragmentation of the sample into tiny (e.g., much less than 1 mm) fragments. Furthermore, examination of the fragments failed to reveal any evidence of consolidation of the fragments like that seen in the fully amorphous LM-1. Increasing the L/D ratio appears to increase the fracture strain further, while the high-speed video of large L/D samples clearly shows multiple fragmentation of the sample. The increased stress to initiate flow, due to the reduction in free volume promoted by annealing, is consistent with the somewhat increased stress obtained in the

high-rate tests compared with those exhibited in the fully amorphous LM-1. The increase in fracture strain appears to occur via the transition of the shear dominated mechanism to one of multiple fragmentation. Multiple fragmentation is often observed in brittle and semi-brittle materials like ceramics and provides a potent energy-absorbing mechanism if the fragments can be contained and further compressed or pulverized. Analysis of the high-speed video of the annealed samples reveals that a similar mechanism may be occurring in these embrittled BMGs that possess high strength. The combination of high strength and increased fracture strain further provides for high energy absorption, whether this occurs via multiple shear banding as observed in the fully amorphous LM-1, or via multiple fragmentation demonstrated by the annealed LM-1.

Finally, the present results may have implications in the design of layered energy-absorbing structures that may utilize BMGs as one or more components. Careful selection of layer thickness and properties will likely affect the tendency to produce shear bands instead of fragmentation, while the constraint provided by other structures may also be beneficial to the energy-absorbing characteristics of systems comprising one or more BMGs. This is a subject of continuing investigation within our group and results will be presented in future publications.

VII. SUMMARY

Split-Hopkinson pressure bar experiments were conducted using cylindrical inserts to investigate the effects of L/D ratio and annealing on the stress, strain-to-failure, and flow/fracture behavior of LM-1 for strain-rates from 500–4000/s. Reductions in the L/D ratio for fully amorphous LM-1 resulted in lower peak stresses but higher apparent strains-to-failure, compared with the larger L/D ratios, because of the consolidation of the original specimen. In situ video recordings showed preferential flow/fracture behavior occurring at the specimen-insert interface, particularly for aspect ratios of 0.5. The annealed LM-1 exhibits slightly increased peak strength and strain-to-failure compared with the fully amorphous material. In situ video recordings showed that the annealed LM-1 initially failed in shear, but the failure mechanism quickly transitioned to multiple fragmentation. A finite element simulation performed to determine the effect of the stress concentration demonstrated stress concentrations in excess of 30%, thereby violating the assumption of a uniform, uniaxial stress state, and that these stress concentrations were more severe for an L/D of 0.5 compared with L/D ratios of 1.0 or 2.0. Based in part by the simulation results, a new insert design was devised to reduce the effect of stress concentrations in the sample. In situ video of experiments with the new inserts captured fracture behavior that showed flow/fracture behavior well removed from the specimen-insert interface for LM-1. The increased compressive strain-to-failure for small-aspect ratios (i.e., $L/D = 0.5$) is consistent with quasi-static experiments performed on specimens with reduced L/D ratios and with superimposed pressure, and the in situ video recordings, combined with other recent work^{21–23} suggest that the stress concentration and associated inhomogeneity of the stress state may, in these experiments, play a dominant role in the final failure of the material that was previously attributed to thermal softening of LM-1.

ACKNOWLEDGMENTS

The authors acknowledge Xin Tang, Fuping Yuan, and Ali Shamimi Nouri for their discussions and experimental support, and Liquidmetal, Inc. for producing and supplying bulk metallic glass plates used in the experiments. The authors also acknowledge Case Western Reserve University (Case Prime Fellowship), the Office of Naval Research (ONR-N00014-03-1-0205), and the Defense Advanced Research Projects Agency (DARPA-ARO-DAAD19-01-0525) for financial support. The authors acknowledge the Major Research Instrumentation award, NSF CMS 0079458 for the acquisition of the high-speed camera used in the present experiments.

REFERENCES

1. A. Peker and W. Johnson: A highly processable metallic glass: $Zr_{41.25}Ti_{13.75}Cu_{12.5}Ni_{10}Be_{22.5}$. *Appl. Phys. Lett.* **63**, 2342 (1993).
2. P. Lowhaphandu and J.J. Lewandowski: Fracture toughness and notched toughness of bulk amorphous alloy Zr-Ti-Ni-Cu-Be. *Scripta Mater.* **38**, 1811 (1998).
3. H.A. Bruck: Quasi-static and dynamic constitutive characterization of beryllium-bearing bulk metallic glasses. Ph.D. Thesis, California Institute of Technology, Pasadena, CA (1994).
4. J. Lu: Mechanical behavior of a bulk metallic glass and its composite over a wide range of strain rates and temperatures. Ph.D. Thesis, California Institute of Technology, Pasadena, CA (2002).
5. T.C. Hufnagel, T. Jiao, Y. Li, L.Q. Xing, and K.T. Ramesh: Deformation and failure of $Zr_{57}Ti_5Cu_{20}Ni_8Al_{10}$ bulk metallic glass under quasi-static and dynamic compression. *J. Mater. Res.* **17**, 1441 (2002).
6. G. Sunny, J.J. Lewandowski, and V. Prakash: Effects of specimen geometry on high strain-rate behavior of a bulk metallic glass, in *Proceedings of the American Society of Mechanical Engineers (IMECE-2005)*, edited by American Society of Mechanical Engineers, Orlando, Florida, November 5–11, 2005.
7. G. Subhash, H. Zhang, and H. Li: Thermodynamic and mechanical behavior of hafnium/zirconium based bulk metallic glasses. In *Proceedings of the International Conference on Mechanical Behavior of Materials (ICM-9)*, edited by American Society of Mechanical Engineers, Geneva, Switzerland, May 25–29, 2003.
8. A.V. Sergueeva, N.A. Mara, J.D. Kuntz, E.J. Lavernia, and A.K. Mukherjee: Shear band formation and ductility in a bulk metallic glass. *Philos. Mag.* **85**, 2671 (2005).
9. C.J. Gilbert, J.W. Ager III, V. Schroeder, R.O. Ritchie, J.P. Lloyd, and J.R. Graham: Light emission during fracture of a Zr-Ti-Ni-Cu-Be bulk metallic glass. *Appl. Phys. Lett.* **74**, 3809 (1999).
10. D. Suh and R.H. Dauskardt: The effect of atomic-scale open-volume on flow and fracture processes in a Zr-Ti-Ni-Cu-Be bulk metallic glass. In *Proceedings of the Fall Materials Research Society Meeting, Boston, MA*, December 2–6, 2002.
11. J.J. Lewandowski: Effects of annealing and changes in stress state on fracture toughness of bulk metallic glass. *Mater. Trans.* **42**, 633 (2001).
12. J.J. Lewandowski, W.H. Wang, and A.L. Greer: Intrinsic plasticity or brittleness of metallic glasses. *Philos. Mag. Lett.* **85**, 77 (2005).
13. J.J. Lewandowski and P. Lowhaphandu: Effects of hydrostatic pressure on flow and fracture of a bulk amorphous metal. *Philos. Mag. A* **82**, 3427 (2002).
14. P. Lowhaphandu: Mechanical behavior of a Zr-based bulk metallic glass. Ph.D. Thesis, Case Western Reserve University, Cleveland, OH (2000).
15. G.T. Gray: Classic Split-Hopkinson Bar testing, in *Mechanical Testing and Evaluation Handbook*, Vol. 8 (American Society for Metals, Materials Park, OH, 2000), pp. 462–476.
16. D. Frew, M. Forrestal, and W. Chen: Pulse shaping techniques for testing brittle materials with a Split Hopkinson pressure bar. *Exp. Mech.* **42**, 93 (2001).
17. G. Subhash and G. Ravichandran: Split-Hopkinson pressure bar testing of ceramics, in *Mechanical Testing and Evaluation Handbook*, Vol. 8 (American Society for Metals, Materials Park, OH, 2000), pp. 497–504.
18. W. Chen, G. Subhash, and G. Ravichandran: Evaluation of ceramic specimen geometries used in a Split-Hopkinson pressure bar. *DYMAT Journal* **1**, 193 (1994).
19. G. Sunny, J.J. Lewandowski, and V. Prakash: Dynamic stress-strain response of $Zr_{41.25}Ti_{13.75}Cu_{12.5}Ni_{10}Be_{22.5}$ bulk metallic glass, in *Proceedings of the Society of Experimental Mechanics*, Portland, Oregon, June 6–9, 2005, Paper 324.

20. B. Yang, C.T. Liu, T.C. Nieh, M.L. Morrison, P.K. Liaw, and R.A. Buchanan: Localized heating and fracture criterion for bulk metallic glasses. *J. Mater. Res.* **21**, 915 (2006).
21. J.J. Lewandowski and A.L. Greer: Temperature rise at shear bands in metallic glasses. *Nat. Mater.* **5**, 15 (2006).
22. Y. Zhang and A.L. Greer: Thickness of shear bands in metallic glasses. *Appl. Phys. Lett.* **89**, 1 (2006).
23. Y. Zhang, N.A. Stelmashenko, Z.H. Barber, W.H. Wang, J.J. Lewandowski, and A.L. Greer: Local temperatures rises during mechanical testing of metallic glasses. *J. Mater. Res.* **22**, 419 (2006).
24. H.A. Bruck, T. Christman, A.J. Rosakis, and W.L. Johnson: Quasi-static constitutive behavior of $\text{Zr}_{41.25}\text{Ti}_{13.75}\text{Ni}_{10}\text{Cu}_{12.5}\text{Be}_{22.5}$ bulk amorphous alloys. *Scripta Metall. Mater.* **30**, 429 (1994).
25. E. Hoek and E.T. Brown: Empirical strength criteria for rock masses. *J. Geotech. Eng.* **106**, 1013 (1980).